J Mater Sci (2013) 48:7456–7465
DOI 10.1007/s10853-013-7560-x

Synthesis, characterization, and performance of a benzimidazole-based membrane in removal of phosphate: first lab-scale experimental results

Bilge Eren · Reyhan Aydın · Erdal Eren

Received: 10 March 2013 / Accepted: 26 June 2013 / Published online: 11 July 2013

Abstract Poly(2,5-benzimidazole) membrane (ABPBI) was investigated for the removal of phosphate species from aqueous solution. This work was conducted to provide fundamental information from the study of equilibrium adsorption isotherms, and to investigate the adsorption mechanisms in the removal of phosphate species using ABPBI. Batch experiments were performed under various conditions of initial phosphate concentration, pH, and contact time. The Langmuir monolayer adsorption capacity of ABPBI was calculated as 87.90 mg/g. The pseudo-first-order kinetic, pseudo-second-order kinetic, and the intra-particle diffusion models were used to describe the kinetic data and rate constants were evaluated. The activation energy for degradation estimated by Kissinger method for ABPBI was found to be 62.6 kJ/mol in air atmosphere. The physicochemical properties of ABPBI were investigated by FT-IR, TGA, and SEM techniques.

Introduction

It was reported that more than 50 % of water eutrophication is attributed to agricultural nutrients, such as phosphates [1]. The USEPA has recommended a limit for controlling eutrophication of 0.05 ppm for total phosphorus in streams that enter lakes and 0.1 ppm for total phosphorus in flowing streams [1]. It is essential to collect the finally disposed phosphates from effluents water before further dispersion of them in the water environment. Various physical, chemical, and biological techniques have been applied to remove dissolved phosphate from wastewater, such as adsorption [2], precipitation–microfiltration [3], and aerobic–anaerobic–anoxic systems [4]. Among these removing techniques, adsorption is known to be more useful and economical.

The removal of phosphate by a membrane bioreactor (MBR) is increasingly under research, and regarded as the wastewater treatment technique of the future [2]. But, maintaining long sludge retention time and retaining high concentration of sludge lead to difficulty in phosphate removal [5]. Ion-exchange/adsorption processes can be developed as post treatment to the MBR. The phosphate can successfully be recovered from the MBR effluent by an ion-exchange/adsorption processes.

It is known that adsorbents should posses high selectivity, high capacity, and long life. Adsorbent structure, surface charge, hydrophobicity, and particle size are the factors influencing adsorbent properties. The phosphates have negative charge, and hence the adsorbent used in their removal processes should posses high positive charge. Poly(2,5-benzimidazole) (ab-PBI or ABPBI; "AB" reflects the fact that the polymer is formed in head–tail variety) as adsorbent is a promising candidate for the removal of phosphates due to its amphoteric behavior, high positive charge, and the ability to form complex or intermolecular hydrogen bonds. Taking all these factors into consideration ABPBI was prepared by condensation of 3,4-diaminobenzoic acid (DABA) monomers in polyphosphoric acid (PPA). To the best of our knowledge, there have been no previous reports on the removal of phosphate ions using a benzimidazole membrane. It is thus necessary to design a set of laboratory scale experimental techniques for a complete characterization of the main removal routes for phosphates using a benzimidazole-based membrane. Since the final goal of this study is to propose an optimal treatment strategy for the removal of phosphates, the complete information on the conventional

B. Eren (✉) · R. Aydın · E. Eren
Department of Chemistry, Faculty of Science and Arts, Bilecik Seyh Edebali University, 11210 Bilecik, Turkey
e-mail: bilge.eren@bilecik.edu.tr

parameters (the removal capability, kinetics, isotherm, and reusability of membrane) and membrane characteristics was followed using lab-scale experiments. The membrane was characterized by infrared spectroscopy (IR) and thermal analysis (TG-DTG), scanning electron microscopy (SEM), X-ray diffraction (XRD) techniques.

Experimental

Preparation of ABPBI membrane

Poly(2,5-benzimidazole) (ABPBI) was prepared by condensation of 3,4-diaminobenzoic acid (DABA) monomers in polyphosphoric acid (PPA) as reported earlier [6, 7]. The polymerization was carried out heating a solution of 3.040 g (20 mmol) of 3,4-diaminobenzoic acid in 50 g of PPA (85 % P_2O_5) at 170 °C for 3 h under nitrogen. The polymer was isolated by precipitation in water, filtered, and washed repeatedly with water. To eliminate residual phosphoric acid, the polymer was washed with 10 % NaOH stirring overnight. The dark purple polymer became brown after the NaOH addition. NaOH was eliminated by washing with water to neutrality and boiling the polymer in water for 6 h, three times. The purified polymer was dried at 100 °C for 24 h and 200 °C for another 24 h. A brown fibrous polymer was obtained. Typical inherent viscosity of a 0.5 g/dL solution was 1.7 dL/g measured in 96 % H_2SO_4 at 30 °C, and was used to estimate the polymer molecular weight, according to the Mark–Houwink equation as given Eq 1 [7].

$$\eta = 8.7 \times 10^{-3} \cdot \mathrm{DP}^{1.10} \quad (1)$$

where DP is the degree of polymerization (DP = Mw/116 for ABPBI). This equation allows us to calculate the polymer molecular weight of 14000 for 1.7 dL/g ABPBI.

Membrane of ABPBI were prepared by evaporation of a methanesulfonic acid solution dissolving 1 g in 15 mL of methanesulfonic acid. Films of this solution were cast on a glass and evaporated at about 200 °C. The membranes were peeled off by immersion in water. The remaining methanesulfonic acid was extracted by washing the membrane in boiling water.

Phosphoric acid doping of the membranes: Samples of about 4 × 4 cm were cut and immersed in different phosphoric acid solutions for 10 min, and dried at 100 °C to eliminate the water absorbed from the doping bath. After a few minutes, a membrane reached almost 100 % of the absorbed maximum acid.

Adsorption/desorption experiments

All reagents were of analytical grade, and all solutions were prepared with double distilled water. Phosphate removal for samples was acquired through batch experiments. The pH of solution was adjusted by 1 mol/L HCl and NaOH and measured with pH meter before the adsorption.

Adsorption studies were performed using batch method. These experiments were conducted in 500 mL glass Erlenmeyer flasks shaken at constant temperature and 200 rpm in a bath shaker. Dried membranes samples were equilibrated in 100 mL solution containing different concentration of phosphate (1.5×10^{-5}–1.5×10^{-4} M NaH_2PO_4) for 4 h at room temperature. A volume of 100 mL of specific phosphate solution was added into the flask, and then a piece of membrane with a surface area 16 cm^2, large enough for sensitive adsorption kinetics experiments, was immersed in the solution. At the end of the 4 h period, the solution was decanted and then analyzed for phosphate concentration (vanadomolybdophosphoric acid colorimetric method). The amount of phosphate sorbed was calculated from the difference between the initial and measured concentrations.

Desorption of phosphate from the spent adsorbent was studied with an aqueous solution of Na_2CO_3 (0.1–1 M). The phosphate loaded ABPBI (0.05 g) was placed in desorption medium and shaken for 4 h at 30 °C. After centrifugation, the supernatant was analyzed for phosphate concentration. Desorption ratio was then calculated from comparison of the initial and final phosphate concentration in the desorption medium.

Characterization methods

Infrared (IR) spectra of the ABPBI samples were recorded in the region 4000–450 cm^{-1} on a Spectrum-100 FTIR spectrometer. The thermal gravimetric (TG) and differential thermal analyses (DTA) curves were obtained using a PRIS Diamond TG/DTG apparatus under static air atmosphere. Surface morphology was studied using a ZEISS Ultraplus model field emission scanning electron microscopy (SEM). The XRD analysis data from the samples were collected using a Rigaku, Miniflex ZD13113 (Japan) diffractometer with Cu Kα radiation (Ni-filter). The electronic spectra were recorded on a Unicam-2 UV–Vis spectrophotometer at 22 ± 1.0 °C using 1 cm matched quartz cells.

Results and discussion

Material characterization

XRD analysis was carried out in order to evaluate the crystallinity of the ABPBI. The XRD pattern of ABPBI prepared in this work is shown in Fig. 1. XRD analysis of

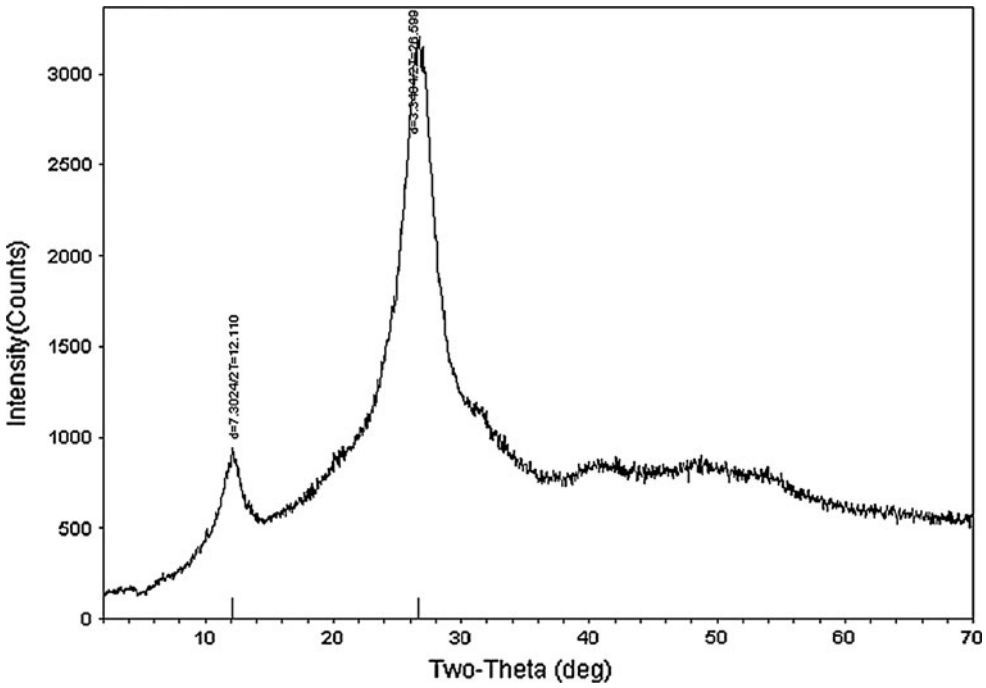

Fig. 1 XRD pattern of ABPBI sample

ABPBI indicated that it was amorphous in nature [8]. ABPBI exhibited two amorphous peaks, indicating that there was two different types of predominant chain packing. A peak corresponding to the lower d-spacing (d_{sp}) of 3.40 Å was dominated by H-bonded region. This reflection arises from planes oriented preferentially parallel to the film surface, and is probably due to planes containing stacked aromatic rings [9]. The peak at higher d_{sp} of 7.3 Å indicated looser chain packing. ABPBI was much lower d_{sp} than that of common polymers like polysulfone [10], polyethersulfone [11], etc. This behavior was attributed to the presence of H-bonding in ABPBI that brings chains closer, resulting in efficient chain packing. SEM images of ABPBI demonstrated that the ABPBI is characterized by an interconnected and highly porous structure (Fig. 2).

In order to better understand the effect of phosphate on the thermal stability of ABPBI, the neat ABPBI and phosphoric acid doped ABPBI (PA–ABPBI) systems with various amounts of phosphoric acid (5–20 wt%) were also analyzed by DTG. Typical TGA curves under air atmosphere for neat ABPBI and PA–ABPBI samples at a heating rate of 10 °C/min are illustrated in Fig. 3, and the related data are listed in Table 1. According to Table 1, thermal degradation occured in two or three stages with various mass percent losses. The thermo-oxidative decomposition of neat ABPBI (Fig. 3a) was a two-step process: first one, the weight loss between 50 and 200 °C was attributed to the water absorbed in ABPBI. Second one, the weight loss in the temperature range of 200–700 °C corresponded to the degradation of ABPBI [12, 13]. As shown in Fig. 3b, the thermal behavior of PA-ABPBI was different from that of ABPBI. The first weight loss corresponded to the loss of absorbed water at about 110 °C. The second weight loss observed from 200 to 300 °C was attributed to the condensation reaction of phosphoric acid to form pyrophosphoric. The last step started at around 600 °C was associated with the continuing dehydration of the pyrophosphoric acid to polyphosphoric acid and the degradation of the ABPBI main chain. At a doping up to 10 wt%, all the curves exhibited almost the same trend. For doping >10 wt%, a new mass loss step was detecteded between 410 and 570 °C. Following this mass loss, a peak about 541 °C was observed in the DTG curve. The intensity of the 541 °C peak increased from 15 to 20 wt% doping. The T_{max} of ABPBI was 555 °C, and increased to 568 °C as the loading increased to 5 wt% PA-content. When 10, 15, and 20 wt% PA are added to the ABPBI matrix, the T_{max} increased to 599, 575, and 569 °C, respectively. The DTA method was studied in static air atmosphere, in order to obtain more information about the thermal transitions occurred. The DTA data are summarized in Table 1. In the case of ABPBI doped with phosphate, there is a broad endothermic peak in the temperature range of 60 and 230 °C, which can be ascribe to the loss of surface absorbed water of ABPBI, of the bound water of ABPBI matrix and condensation of phosphate groups to give pyrophosphoric and then polyphosphoric acid, respectively. The exothermic peak was observed at 555 °C in the case of ABPBI, whereas that for 10, 15, and 20 wt% PA doped ABPBI was observed at 568, 598, 575, and 569 °C, respectively. The studies related to the role of oxygen on the degradation of polymers showed that oxygen

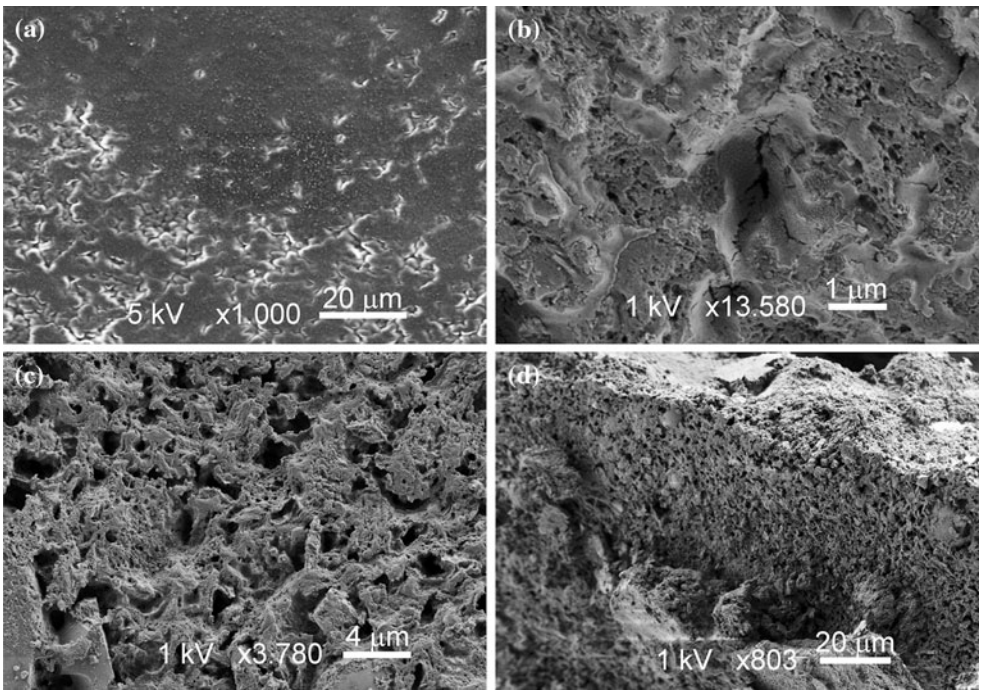

Fig. 2 The SEM images of ABPBI at different magnifications: raw ABPBI (**a**) and after applying for phosphate removal (**b–d**)

initiates the degradation of polymers leading to the formation of hydroperoxides yielding char. In this degradation process, the reaction of oxygen with the polymeric matrix initiates earlier degradation of the polymer and stabilize char at high temperatures [14, 15]. In this study, enhanced DTA temperature values suggested that PA promoted thermal stability and char yielding during the thermo-oxidative degradation of the ABPBI.

The thermo-oxidative degradation activation energy of sample was calculated by Kissinger method according to the TGA data, which were measured under air at different heating rates: 2.5, 5, 10, 15, and 20 °C/min [16]. The Kissinger method was utilized to analyze the TGA data because it is independent of any pre-assumption about the thermal degradation mechanism. The activation energy for ABPBI was calculated from the linear dependence of the $\ln(\beta/T_{\max}^2)$ versus $1/T_{\max}$ plot (not shown) for various heating rates, according to Eq. (2).

$$\ln\left(\frac{\beta}{T_{\max}^2}\right) = \left(\ln\frac{AR}{E_a}\right) - \frac{E_a}{RT_{\max}} \quad (2)$$

In the above equation, A is the pre-exponential factor, E_a is the apparent activation energy of the degradation reaction, R is the universal gas constant, β is the heating rate. The activation energy was calculated from the $T_{\max}$, the temperature at which the maximum degradation occurs for different heating rates by assuming that weight loss percentage at $T_{\max}$ is constant. The E_a for degradation of ABPBI found to be 62.6 kJ/mol under static air atmosphere. These values fall within the range of activation energies for ABPBI degradation reported previously [12, 13].

Adsorption isotherms and parameters

Langmuir model

The equilibrium data have been analyzed using the Langmuir model, and the characteristic parameters for this isotherm have been determined [17]. The data conformed to the linear form of the Langmuir model [17] (Eq. 3) expressed below:

$$C_e/q_e = C_e/q_m + 1/K_L q_m \quad (3)$$

where C_e is the equilibrium concentration of phosphate (mg/L) and q_e is the amount of the phosphate adsorbed (mg) per unit of ABPBI (g). q_m and K_L are the Langmuir constants related to the adsorption capacity (mg/g) and the equilibrium constant (L/g), respectively. Linear plots of C_e/q_e versus C_e (not shown) were employed to determine the value of q_m (mg/g) and K_L (L/mg). The parameters obtained from Langmuir model is presented in Table 2. The regression coefficient obtained from the Langmuir model ($R^2 = 0.986$) suggested the applicability of the Langmuir model. There are few studies related to phosphate adsorption on polymers [18]. The Langmuir monolayer adsorption capacitiy for ABPBI sample, was calculated as 87.90 mg/g at 298 K, is compatible with

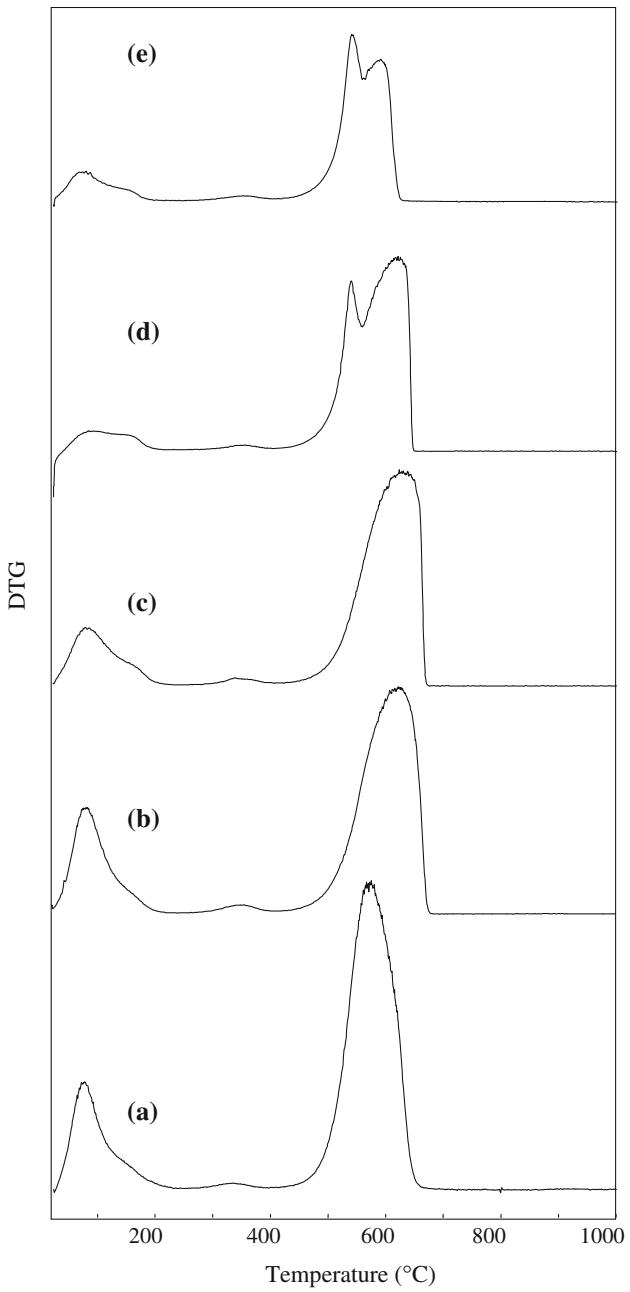

Fig. 3 TG curves of ABPBI and various amounts of phosphoric acid-doped ABPBI samples obtained at a heating rate of 10 °C min^{-1} under air atmosphere

reported values in the literature. For example, Kavakli et al. [18] reported that q_m for adsorption of phosphate on dimethylaminoethylmethacrylate grafted polyethylene/polypropylene sample is 63 mg/g. In this study, maximum adsorption capacity calculated from the Langmuir isotherm was also much higher than literature values reported for different adsorbents. For example, adsorption of phosphate on $ZnCl_2$-activated carbon follows the Langmuir isotherm model with an adsorption capacity of 5.1 mg/g [19]. Langmuir adsorption capacity for phosphate adsorption on Clay-T, Clay-G, and Zeolite-70 °C was shown to be 38.46, 42.19, and 52.91 mg/g, respectively, by Hamdi and Srasra [20]. Rodrigues and Silva [21] found monolayer capacity as 15 mg/g for phosphate adsorption on niobium oxide. The uptake of phosphate on Al–Bentonite, Fe–Bentonite, and Fe–Al–Bentonite has Langmuir monolayer capacity of 12.7, 11.2, and 10.5 mg/g, respectively [22]. Langmuir adsorption capacity for phosphate on natural palygorskite was found as 3.7 mg/g by Ye et al. [23]. The high adsorption capacity of ABPBI proved that ABPBI could be used as potential adsorbent for the removal of phosphate ions in adsorption columns.

Freundlich model

The adsorption equilibrium data was also applied to the Freundlich model [24] (Eq. 4) given below:

$$\log q_e = \log K_F + (1/n) \log C_e \quad (4)$$

where K_F and n are the Freundlich constants related to adsorption capacity and adsorption intensity, respectively. Linear plots of log C_e versus log q_e (not shown) were employed to determine the value of n and K_F ((mg/g)(L/mg)$^{1/n}$). In this adsorption model, K_F is related with adsorption capacity, and n is a measure of the intensity of adsorption [25–27]. $n \ll 1$ means that adsorption intensity is favorable over the entire range of concentrations studied, whereas $n > 1$ indicates that adsorption intensity is favorable at high concentrations [26, 27]. In this study, the Freundlich constants K_F and n were found to be 7.05 and 2.13, respectively. The high value of n indicated a strong bond between the adsorbent and the adsorbate, a desired parameter in adsorption process (Table 3). The high K_F Freundlich parameter value indicated a high affinity of phosphate ions onto the ABPBI.

Phosphate adsorption kinetics

Several kinetic models are available to understand the behavior of the adsorbent, and also to examine the controlling mechanism of the adsorption process and to test the experimental data. In the present investigation, the adsorption data were analyzed using three kinetic models, the pseudo-first order, pseudo-second order kinetic, and the intra-particle diffusion models.

The pseudo-first order model was presented by Lagergren [28]. The Lagergren's first-order reaction model is expressed as follows:

$$\log(q_e - q_t) = \log q_e - (k_1/2.303)t \quad (5)$$

where q_e and q_t are the amounts of dye (mg/g) adsorbed on the ABPBI at equilibrium, and at time t, respectively and k_1 is the rate constant (min^{-1}). The rate constant, k_1 was

Table 1 TG/DTA characteristics of ABPBI and various amounts of phosphoric acid doped ABPBI

Material	Thermal degradation step	T_{onset} (°C)	T_{endset} (°C)	W (%)	DTA charateristic	Residue (%)[a]
Neat ABPBI	I	61	140	14.69	Endothermic	1.6
	II	410	670	77.04	Exothermic	
5 wt% PA/ABPBI	I	69	180	17.2	Endothermic	2.1
	II	410	690	69.2	Exothermic	
10 wt% PA/ABPBI	I	64	230	13.3	Endothermic	2.3
	II	430	690	31	Exothermic	
15 wt% PA/ABPBI	I	64	230	6.0	Endothermic	2.4
	II	410	581	28.8	Exothermic	
	III	590	65.5	28.5	Exothermic	
20 wt% PA/ABPBI	I	59	180	6.7	Endothermic	2.6
	II	410	570	25.6	Exothermic	
	III	570	630	17.5	Exothermic	

[a] The loading PA amount was subtracted

Table 2 Langmuir and Freundlich isotherm parameters for the adsorption of phosphate onto ABPBI

Langmuir constants			Freundlich constants		
q_m (mg/g)	K_L (L/mg)	R^2	n	K_F ((mg/g)(L/mg)$^{1/n}$)	R^2
87.90	0.025	0.986	2.13	7.05	0.945

obtained from slope of the linear plots of $\log(q_e - q_t)$ against t.

The adsorption data was also analyzed in terms of pseudo-second-order mechanism, described by Ho and McKay [29].

$$t/q_t = (1/h) + (1/q_e)t \quad (6)$$

and the initial rate of adsorption h is:

$$h = k_2 q_e^2 \quad (7)$$

where k_2 is the rate constant of pseudo-second-order adsorption (g/mg min), h is the initial rate of adsorption (mg/g min). If second-order kinetics is applicable, the plot of t/q_t against t of Eq. (5) should give a linear relationship from which the constants q_e, h, and k_2 can be determined.

The results of the rate constant studies for different initial phosphate concentrations by the pseudo-first-order and pseudo-second-order models at 298 K are listed in Table 3. It is seen that the correlation coefficients of pseudo-first-order kinetic are lower than in the case of pseudo-second-order kinetic model. This finding showed that kinetics of phosphate adsorption by ABPBI were better described by pseudo-second-order kinetic model rather than pseudo-first-order model. As given in Table 3, the rate constant of phosphate uptake was found to decrease from 3.6×10^{-2} to 0.60×10^{-2} g/mg min for ABPBI with the increase of the initial phosphate concentration from 25 to 500 mg/L. At lower concentrations, phosphate ions presented in the adsorption medium could interact with the binding sites, hence higher rate constant results. At higher concentrations, because of the saturation of the adsorption sites, the rate constant of the phosphate by the polymer showed a decreasing trend.

In adsorption systems where there is the possibility of intra-particle diffusion being the rate-limiting step, the intraparticle diffusion approach described by Weber and Morris [30] can be used. This equation can be described as (Eq. 8)

$$q_t = k_d t^{1/2} + C \quad (8)$$

where q_t is the amount of phosphate adsorbed (mg/g) at time t, k_d (mgl/g min$^{1/2}$) is the rate constant for intra-particle diffusion, and C is the intercept.

Table 3 Kinetic parameters for the adsorption of phosphate onto ABPBI. Contact time 240 min, initial pH 5, and $m = 1$ g/L

C_o (mg/L)	Pseudo-first order model		Pseudo-second order model			Intra-particle diffusion model		
	k_1 (min^{-1})	R_1^2	R_2^2	$q_{e,cal}$ (mg/g)	$k_2 \times 10^2$ (g/mg min)	k_i (mg/g min$^{1/2}$)	C (mg/g)	R_i^2
25	0.005	0.719	0.999	19.97	3.6	0.18	17.52	0.946
500	0.001	0.919	0.999	471.57	0.6	0.60	461.72	0.841

The values k_i, C, and correlation coefficient calculated from the slope of the plot of q_t versus $t^{1/2}$ are shown in Table 3. It was found that the correlation coefficient for the intraparticle diffusion model was lower than that of the pseudo-second-order model. As given in Table 3, it is obvious that values of k_i increased from 0.18 to 0.60 mg/g $min^{1/2}$ when the initial phosphate concentration was increased from 25 to 500 mg/L. On the other hand, if the q_t versus $t^{1/2}$ plot is linear and passes through the origin, then intraparticle diffusion is the sole rate-limiting step [31, 32]. The regression was linear, but the plot was not pass through the origin (the values of the intercept in Table 3), suggesting that adsorption involved intraparticle diffusion, but that was not the only rate-controlling step. Other kinetic models may control the adsorption rate. It was also observed that the value of the intercept increased from 17.52 to 461.5 mg/g, which indicated that the thickness of the boundary layer increased significantly with increase of initial phosphate concentration [33]. The values of the intercept (C in Table 3) also give an idea about the boundary layer thickness: the larger the intercept, the greater is the boundary layer effect. Namely, any increase in the value of C indicates the abundance of solute adsorbed on boundary layer. As seen in Table 3, the value of C increases with increasing concentration. It showed that deviations from intraparticle diffusion kinetic model mainly occurred at high initial phosphate concentration (Table 3). These deviations were attributed to some repulsion between phosphate–phosphate ions and/or adsorbent/adsorbate molecules due to concentration density. Comparing the correlation coefficients for this system in this study, the calculated correlation coefficients of phosphate are closer to unity for pseudo-second-order kinetic model than those for the other models. Therefore, the adsorption can be approximated more appropriately by the pseudo-second-order kinetic model than the other models. This trend suggests that a chemisorption reaction or an activated process can be more predominant in the rate-controlling step [34].

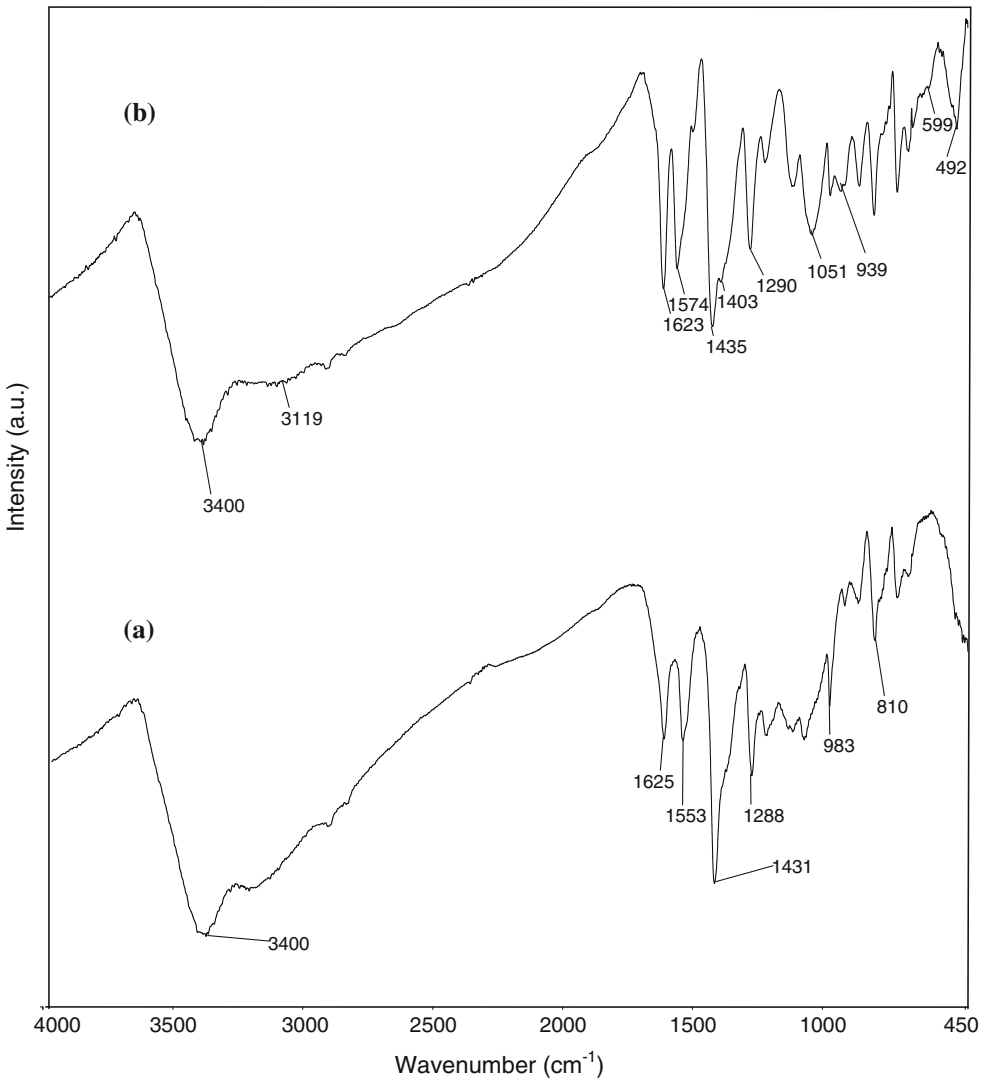

Fig. 4 IR spectra of ABPBI **a** raw ABPBI, **b** after applying for phosphate removal

Adsorption mechanism of phosphate onto ABPBI

ABPBI showed the characteristic absorption band at 3450–3250 cm^{-1} (N–H stretching), 1625 (C=N stretching), and 1553 cm^{-1} (C=C stretching of of aromatic ring) (Fig. 4a). The presence of a benzimidazole group was confirmed by the characteristic bands at 1430 cm^{-1} due to the inplane deformation of the benzimidazole rings. The band at 1431 cm^{-1} was attributed to the inplane deformation of benzimidazole rings. The band at 1288 cm^{-1} was assigned to the breathing mode of the imidazole ring in ABPBI. In the spectrum of ABPBI adsorbed phosphate (Fig. 4b), four additional vibration bands were observed at 1051, 939, 599, 489 cm^{-1} corresponding to different modes of the phosphate groups [35–37]. The band at 1084 cm^{-1} shifted to 1051 cm^{-1} and broadened. Broadening band at 1051 cm^{-1} showed the presence of the phosphate group and its interaction with the polymer [35–37]. The ABPBI adsorbed phosphate also exhibited a broad absorption peak at 3300–2900 cm^{-1} as well as a shoulder peak at 1403 cm^{-1}, which were ascribed to the protonated N–H and C=N stretching vibrations, respectively. Moreover, ABPBI adsorbed phosphate displayed more intense bands at 1625 and 1439 cm^{-1} than ABPBI indicating strong hydrogen bonding.

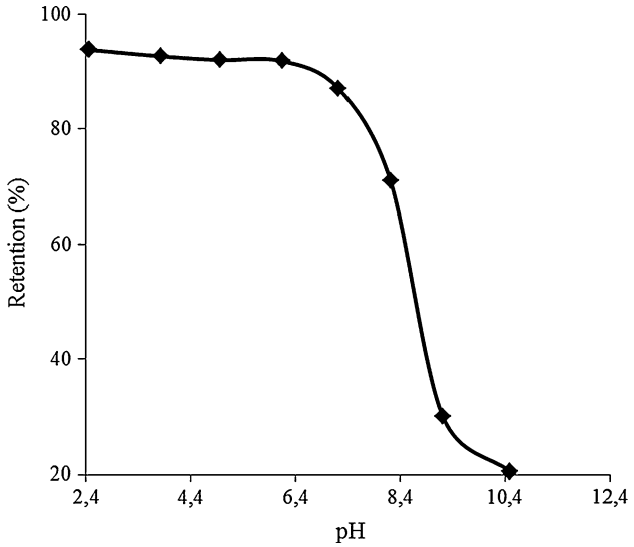

Fig. 5 Adsorption of phosphate (25 mg/L) by ABPBI (1 g/L) as function of pH

Phosphate can exist in different ionic species such as monovalent $H_2PO_4^-$, divalent HPO_4^{2-}, and trivalent PO_4^{3-} ions, depending on the pH of the solution ($pK_1 = 2.15$, $pK_2 = 7.20$, $pK_3 = 12.33$). The pH is a critical criterion for determining the surface characteristics of adsorbents and the adsorption/desorption equilibrium of adsorbates. When pH of the solution is higher than the point of zero charge (pH_{PZC}), the positive charge on the surface provides electrostatic interactions that are favorable for adsorbing anionic species. The total amount of phosphate adsorbed under different pH values is shown in Fig. 5. Adsorption capacity was significantly higher at pH 3.0, but relatively stable in the pH range of 4.5–6.0. In subsequent phosphate adsorption studies, the pH of the solutions was adjusted to 3.1. The value of pKa of polybenzimidazole reported in the literature was close to 5.5 [38]. Phosphate uptake by PBI decreased with an increase in pH; this can be ascribed to effect of a decrease in protonated sites of imidazole ring. In order to take up phosphate, imidazole ring was protonated by accepting proton from $H_2PO_4^-$ and HPO_4^{2-} species. Above pH 6.5, the dominat form of phosphate is HPO_4^{2-}, which is not strong enough to protonate the imidazole ring [$pK_2 > pK_a$(PBI)]. Based on the above analysis, it was considered that the strong hydrogen bonding should be the dominating adsorption mechanism for phosphate onto ABPBI. The stronger hydrogen bonds were formed between N atoms and phosphate species than that of between N atoms and –NH groups, as a result of the acidities of H_3PO_4 and $H_2PO_4^-$. The ABPBI can only remove H_3PO_4 and $H_2PO_4^-$ species, on the basis of Fig. 5 results. At pH values >6.5, the imidazole group lose a hydrogen (become

Fig. 6 The plausible mechanisms about adsorption of phosphate onto ABPBI

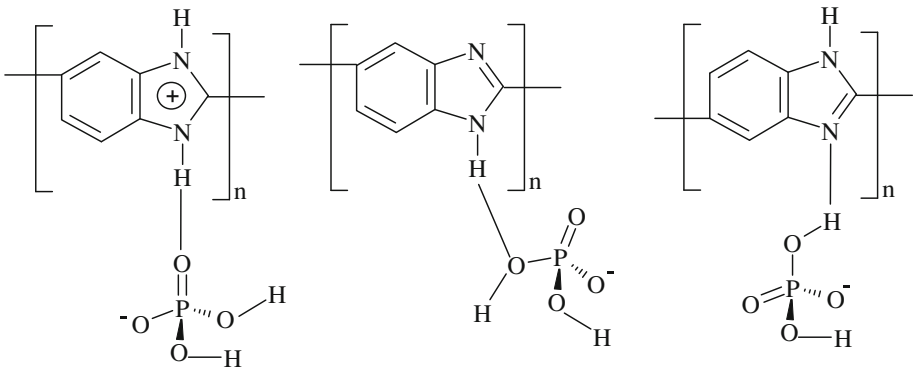

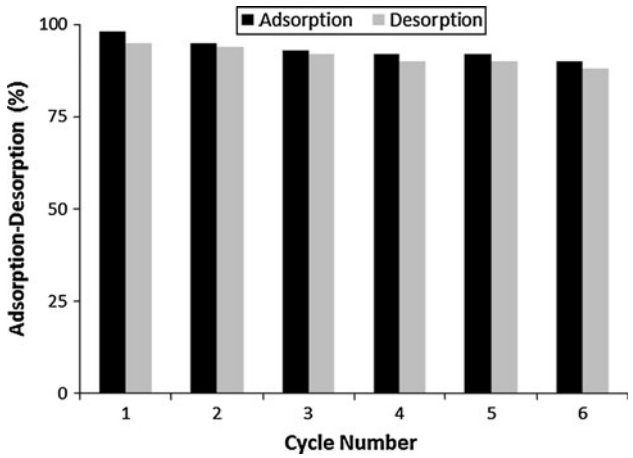

Fig. 7 Adsorption–desorption experiments on phosphate ions onto ABPBI. Adsorbent amount: 1 g/L, contact time: 2 h, $T = 298$ K

deprotonated) and exist in its uncharged N-form. At pH values >6.5, the ABPBI gets more and more deprotonated and the overall ionic interactions become weaker. Coulombic attraction and hydrogen bonding was the predominant process of phosphate removal. The plausible mechanisms about adsorption of phosphate onto ABPBI is shown in Fig. 6.

Reusability of ABPBI

Desorption is an important process in adsorption studies because it enhances the economical value of adsorption process. Desorption efficiency of the spent adsorbent was checked with different concentrations of Na_2CO_3 (0.1–1 M). Almost 99.2 % adsorbed phosphate was desorbed from the spent adsorbent using 1 M Na_2CO_3, and hence it was used to regenerate ABPBI. The adsorption–desorption cycle was repeated six times with same adsorbent using 1 M Na_2CO_3, and the results are represented in Fig. 7. Although there was a slight decrease in the adsorption capacities with regeneration cycles (from 99.6 to 90.2 %), the spent adsorbent still possessed high adsorption capacity, and hence the adsorbent can be used for multiple cycles. The regeneration of adsorbent with 1 M Na_2CO_3 showed that the adsorption–desorption process using ABPBI was a reversible process. This showed the great potential applications of ABPBI for the removal of phosphate.

Conclusion

The removal of the phosphate as well as its recovery from water and wastewater is a major issue in these days. Adsorption tests were conducted in batch reactors to study the adsorption behavior of phosphate using ABPBI membrane. It was concluded that ABPBI can be considered as a promising membrane for phosphate removal from aqueous media containing H_3PO_4 and $H_2PO_4^-$ phosphate species. The adsorption isotherm studies indicated that the adsorption of ABPBI followed both the Langmuir and Freundlich isotherms. The experimental kinetic data were modeled using the pseudo-first-order and pseudo-second-order kinetic equations. The strong hydrogen bonds between N atoms and phosphate species were formed as a result of the acidities of phosphate species. Coulombic attraction and hydrogen bonding was the predominant process of phosphate removal.

References

1. U.S. Environmental Protection Agency, Quality criteria for water (1986) Washington, DC, U.S. Environmental Protection Agency Report 440/5-86-001, Office of Water
2. Genz A, Kornmüller A, Jekel M (2004) Water Res 38:3523
3. Katz I, Dosoretz CG (2008) Desalination 222:230
4. Lu NC, Liu JC (2010) Sep Purif Technol 74:329
5. Kim H-G, Jang H-N, Kim H-M, Lee D-S, Chung T-H (2010) Desalination 250:629
6. Linares JJ, Sanches C, Paganin VA, González ER (2012) J Electrochem Soc 159(7):F194
7. Asensio JA, Borrós S, Gómez-Romero P (2004) J Electrochem Soc 151(2):A304
8. Kumbharkar SC, Kharu UK (2010) J Membr Sci 360:418
9. Cho J, Blackwell J, Chvalun SN, Litt M, Wang Y (2004) J Polym Sci Polym Phys 42:2576
10. Dai Y, Guiver MD, Robertson GP, Kang YS, Lee KJ, Jho JY (2004) Macromolecules 37:1403
11. Khayet M, Garcia-Payo MC (2009) Desalination 246:121
12. Asensio JA, Borrós S, Gómez-Romero P (2004) Electrochim Acta 49:4461
13. Asensio JA, Borrós S, Gómez-Romero P (2004) J Membr Sci 241:89
14. He Q, Song L, Hu Y, Zhou S (2009) J Mater Sci 44:1308. doi:10.1007/s10853-009-3266-5
15. Bourbigot S, Gilman JW, Wilki CA (2004) Polym Degrad Stab 84:483
16. Kissinger HE (1957) Anal Chem 11:1702
17. Langmuir I (1918) J Am Soc 40:1361
18. Akkas-Kavaklı P, Kavaklı C, Guven O (2010) Radiat Phys Chem 79:233
19. Namasivayam C, Sangeetha D (2004) J Colloid Interface Sci 280:359
20. Hamdi N, Srasra E (2012) J Environ Sci 24:617
21. Rodrigues LA, Caetano Pinto da Silva ML (2010) Desalination 263:29
22. Yan L, Xu Y, Yu H, Xin X, Wei Q, Du B (2010) J Hazard Mater 179:244
23. Ye H, Chen F, Sheng Y, Sheng G, Fu J (2006) Sep Purif Technol 50:283
24. Freundlich H (1906) Zeitschrift für Physikalische Chemie (Leipzig) 57:385
25. Zhou Y, Jin Q, Hu X, Zhang Q, Ma T (2012) J Mater Sci 47:5019. doi:10.1007/s10853-012-6378-2
26. Liu M, Liu H, Bai L, Liu Y, Cheng J, Yang G (2011) J Mater Sci 46:4820. doi:10.1007/s10853-011-5392-0

27. Hameed BH, Ahmad AL, Latif KNA (2007) Dyes Pigments 75:143
28. Lagergren S (1898) Kungliga Svenska Vetenskapsakademiens Handlingar 24:1
29. Ho YS, McKay G (1999) J Environ Sci Health A 34:1179
30. Weber WJ, Morris JC (1963) J Sanit Eng Div Am Soc Civ Eng 89:31
31. Al-Ghouti M, Khraisheh MAM, Ahmad MNM, Allen S (2005) J Colloid Interface Sci 287:6
32. Mall ID, Srivastava VC, Kumar GVA, Mishra IM (2006) Colloids Surf A 278:175
33. Kannan N, Sundaram MM (2001) Dyes Pigments 51:25
34. Zhao Y-G, Shen H-Y, Pan S-D, Hu M-Q, Xia Q-H (2010) J Mater Sci 45:5291. doi:10.1007/s10853-010-4574-5
35. Elzinga EJ, Sparks DL (2007) J Colloid Interf Sci 308:53
36. Zhang J, Shen Z, Mei Z, Li S, Wang W (2011) J Environ Sci 23:199
37. Arai Y, Sparks DL (2001) J Colloid Interface Sci 241:317
38. Asensio JA, Sánchez EM, Gómez-Romero P (2010) Chem Soc Rev 39:3210